Nanotechnology, Science and Applications

Dovepress
Taylor & Francis Group

Open Access Full Text Article

ORIGINAL RESEARCH

Characterization of Alpha Mangostin Loaded-Mesoporous Silica Nanoparticle and the Impact on Dissolution and Physical Stability

Diah Lia Aulifa[1], Annisa Hafizhah Saepudin[1], Priskila Margaretha[1], Miski Aghnia Khairinisa[2], Arif Budiman[3]

[1]Department of Pharmaceutical Analysis and Medicinal Chemistry, Faculty of Pharmacy, Padjadjaran University, Sumedang, 45363, Indonesia; [2]Department of Pharmacology and Clinical Pharmacy, Faculty of Pharmacy, Universitas Padjadjaran, Sumedang, 45363, Indonesia; [3]Department of Pharmaceutics and Pharmaceutical Technology, Faculty of Pharmacy, Universitas Padjadjaran, Sumedang, 45363, Indonesia

Correspondence: Diah Lia Aulifa, Department of Pharmaceutical Analysis and Medicinal Chemistry, Faculty of Pharmacy, Universitas Padjadjaran, Jl. Raya Bandung-Sumedang Km. 21, Bandung, 45363, Indonesia, Email diah.lia@unpad.ac.id

Purpose: Improving drug solubility is crucial in formulating poorly water-soluble drugs, especially for oral administration. The incorporation of drugs into mesoporous silica nanoparticles (MSN) is widely used in the pharmaceutical industry to improve physical stability and solubility. Therefore, this study aimed to elucidate the mechanism of poorly water-soluble drugs within MSN, as well as evaluate the impact on the dissolution and physical stability.

Methods: Alpha mangostin (AM) was adopted as a model of a poorly water-soluble drug, while MSN with the pore size of 45 Å (MSN45) and 120 Å (MSN120) were used as Mesoporous materials. AM-loaded MSN (AM/MSN45 and AM/MSN120) was prepared by solvent evaporation method.

Results: The amorphization of AM/MSN45 and AM/MSN120 was confirmed by the halo pattern observed in the powder X-ray diffraction pattern and the absence of the melting peak and the glass transition of AM in the DSC curves. This signified the successful incorporation of AM into MSN. FT-IR measurements suggested the formation of hydrogen bond interaction between the carbonyl group of AM and the silica surface of MSN. In the dissolution test, the presence of the AM within MSN improved the dissolution rate and generated the supersaturation of AM. However, the difference of pores size of MSN could affect the dissolution profile of AM within MSN. Additionally, it retained the X-ray halo patterns after 30 d of storage at 25 ^{o}C and 0% RH.

Conclusion: In conclusion, AM-loaded mesoporous silica significantly improved the dissolution and physical stability.

Keywords: mesoporous silica, alpha mangostin, amorphization, dissolution, physical stability

Introduction

The Alpha-mangostin (AM) is a major xanthone in fruit pericarps, bark and dried sap of the mangosteen tree (*Garcinia mangostana* Linn). AM has various pharmacological activities, including antioxidant, anticancer and anti-inflammatory activities.[1–5] More importantly, AM exhibits strong antimicrobial activity against various pathogens, such as methicillin-resistant *Staphylococcus aureus*,[5,6] vancomycin-resistant *Enterococci*[5,7] and acne-inducing *Propionibacterium acnes* (*P. acnes*),[5,8,9] which is recently renamed as *Cutibacterium acnes* (C. acnes).[5,10,11] Consequently, AM has recently been used either as a substitution or as an adjuvant for antibiotics in the treatment of some infectious diseases, especially *Acnes vulgaris*, to decrease problems arising from antibiotic overuse.[5,12,13] However, it has a low water solubility leading to poor bioavailability, as drug molecules need to dissolve in the gastrointestinal fluid for absorption in the intestines.[14–16] The poor bioavailability poses a significant challenge in developing oral dosage forms for AM.[17] Therefore, strategies to improve drug solubility are particularly necessary for oral administration.[18,19]

Amorphization is a promising strategy to improve the solubility, dissolution rate, and bioavailability of poorly water-soluble drugs. Amorphous drugs pose higher Gibbs free energy compared to their crystalline counterparts, which

Received: 2 October 2024
Accepted: 23 December 2024
Published: 9 January 2025

enhances aqueous solubility and achieves high concentrations in water.[20] This can lead to the improvement of oral bioavailability.[21] However, developing solid formulations for amorphous drugs with-out excipients or carriers is practically difficult due to thermodynamic instability and the tendency to recrystallize during storage or after dispersion in water.[22] Therefore, the addition of an excipient or carrier is needed for stabilization.

Drug-loaded-mesoporous silica nanoparticles (MSN) are a promising strategy to inhibit recrystallization.[23] Amorphous drugs can be stabilized by encapsulation into the nanoparticles, which leads to an improvement in the in vitro dissolution rate and apparent solubility.[20,24,25] Drug crystallization within MSN can be prevented using 2 mechanisms. The first is molecular interaction between the surface of MSN and the functional groups of the drug molecules, leading to monomolecular adsorption. The second mechanism is the nanoconfinement effect, in which the pores size of the nanoparticles is smaller compared to critical crystalline nuclei, leading to the suppression of crystal growth.[26,27] This signified that surface area and pore volume could affect the inhibition of the drug crystallization.[28,29]

The formulation of the drug-loaded MSN carriers has been extensively investigated.[30] However, the characterization of AM-loaded-MSN has not been studied. The mechanism of each drug within the nanoparticles would be different due to unique physicochemical properties.[28] Consequently, the impact on dissolution rate, physical stability, and bioavailability can differ for each drug.[31–34] This study was conducted to investigate the characterization of AM loaded-MSN and its relationship with dissolution profile and physical stability. Understanding the mechanism of AM within MSN as well as its impact on pharmaceutical properties is necessary for optimizing the formulations, specifically for oral administration.

Materials and Methods

Materials

The AM (MW = 410.5 g/mol) was purchased from Chengdu BioPurify Phytochemicals Ltd., China (Cat. No.: BP0773). Furthermore, MSN with pore diameter 45.0 Å (MSN45) and 120.0 Å (MSN120) were supplied by Sigma-Aldrich (Singapore). Methanol, Na_2HPO_4, and Na_2HPO_4 were obtained from Merck, while other chemicals were of reagent grade.

Estimation of AM Molecular Dimension

A single crystal structure of AM was collected from PubChem with the CID 5281255. The compound was prepared using Chem3D Pro 12.0. The "measure distance" tool was used to determine the distance between the atoms. Subsequently, the surface area for adsorption was estimated from the 2 longest dimensions of the AM structure.

Calculation of the Theoretical Monolayer of the AM Structure

The quantity of AM needed to obtain the monolayer coverage within MSN particles was calculated in accordance with the procedures of Azaïs et al[35] as shown in the following Equation (1)

$$X = \frac{SSA_{MSN} \times 10^{22} \times MW_{drug}}{S_{drug} \times N_a} \quad (1)$$

where, X shows the capacity of AM needed to form the monolayer adsorption on the silica surface of MSN (g/g), SSA_{MSN} is the specific surface area (SSA) of MSN (MSN45 = 1040 m^2/g and MSN120 = 473 m^2/g), MW_{drug} is the weight of the drug molecule (AM = 410.5 g/mol), S_{drug} is the molecular contact surface area of each drug, and NA is the number of Avogadro (6.022×10^{23} mol^{-1}). The molecular dimensions of AM were estimated as shown in Figure 1.

Preparation of AM Loaded-MSN by Solvent Evaporation Method

AM-loaded MSN was prepared using the solvent evaporation method. Initially, the compound was dissolved in methanol was used to dissolve AM, and MSN was dispersed into the solution. The suspension was sonicated at 25 °C for 3 min and evaporated for 15 min at 40 °C using a rotary evaporator with a water bath. The resulting powder was dried at 40 °C for 48h in an oven to obtain AM-loaded MSN (AM/MSN45 and AM/MSN120).

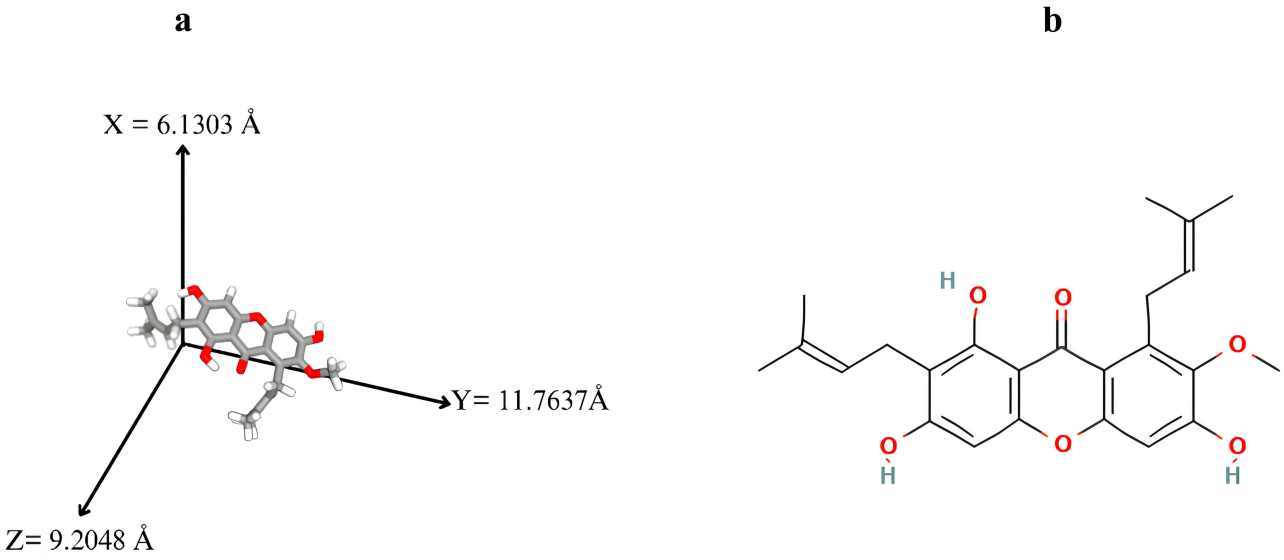

Figure 1 Molecular structure and estimated molecular dimensions of AM (**a**) 3D, and (**b**) 2D.

Powder X-Ray Diffraction (PXRD) Measurement

PXRD measurement was performed using The PANalytical X'Pert PRO series PW3040/X0 to evaluate the drug crystallinity in the AM/MSN. The set conditions were the target, Ci; filters, Ni; 40 kV voltage, 40 mA current, 4°/min scamming rate, and 2θ=4°-60°C scanning angle.

Differential Scanning Calorimetry (DSC) Measurement

DSC measurement was conducted using a Shimadzu 60 DSC instrument. An aluminum pan containing a 5 mg sample was filled with N_2 and purged at a flow rate of 10 °C /minute. Subsequently, the sample was measured at a temperature of 0–200 °C and a heating speed of 2 °C/min with a modulation of ± 0.5 °C.

Fourier Transform-Infrared (FT-IR) Spectroscopy

The FT-IR spectrometer (Shimadzu IRPrestige 21) was used to record the IR spectra of samples. For the analysis, 4 mg of each sample was mixed with 100 mg KBr, compressed into tablets, and scanned from 400–4000 cm^{-1} region.

Drug Loading Efficiency Measurement

The drug loading efficiency of AM loaded-MSN was determined by adding AM/MSN in methanol and stirring for 1 h. Subsequently, 5 mL of the supernatant was filtered through a 0.45 µm membrane filter and analyzed using high-performance liquid chromatography (HPLC).

HPLC Condition

The HPLC analysis was conducted with a Dionex-Ultimate 3000 hPLC instrument (Dionex, Sunnyvale, CA, USA). The sample was injected into an Inertsil ODS C18 (Torrance, California, USA) column sized 6.0×150 mm at an ambient temperature of 30 °C. The mobile phase consisted of a mixture of acetonitrile and 0.1% formic acid in water, with a ratio of 95:5. The samples were identified utilizing a UV detector set at a wavelength of 244 nm.

Crystalline and Amorphous Solubility Measurement

The solubility of AM crystal and AM/MSN was determined using 50 mm phosphate buffer at pH 7.4 and 37 °C. The excess amount of each sample was dispersed into the phosphate buffer solution and shaken for 48 h at 37 °C. Subsequently, the solutions were filtered through a 0.45 µm membrane filter, diluted with methanol, and analyzed using HPLC. Amorphous solubility of AM was also determined using centrifugation, as described in a previous report by Dening et al.[36]

https://doi.org/10.2147/NSA.S499007

Dissolution Test

AM crystal and AM loaded-MSN were dissolved using the paddle method with Sotax AG CH-4008 dissolution instrument under non-sink conditions. The powder samples at an AM concentration of 50 μg/mL were dispersed in 300 mL 50 mm phosphate buffer at pH 7.4. The solution was stirred at 37 °C with a paddle rotating at 150 rpm. Subsequently, 3 mL of dissolution media was withdrawn at definite time intervals, filtered through a 0.45-μm membrane filter, diluted with methanol, and analyzed using HPLC. The first filtrate around 0.15–0.2 mL was discarded after the filtration process.

Physical Stability

The physical stability of AM/MSN was evaluated by storing each sample under different conditions. These include (a) 25 ºC in a tightly capped vial (0% relative humidity (RH)), as well as (b) 20 °C and 95% relative humidity (RH) in a desiccator containing saturated potassium nitrate solution.[37] Finally, samples were evaluated via PXRD after a 14-day storage.

Results

PXRD Measurement

Figure 2 shows the PXRD pattern of AM/MSN with various weight ratios. Crystalline AM presented characteristic peaks of crystalline in the PXRD pattern, while the MSN45 and MSN120 featured a halo pattern. The characteristic diffraction peaks were observed as well in the AM produced by solvent evaporation (AM SE), suggesting that the amorphous state of AM did not occur as a result of its strong tendency to recrystallize. The AM/MSN45 at the ratio of 7:3 and 5:5 showed distinct peaks belonging to the compound, signifying the existence of crystals in the samples, while no peaks were observed at the ratio of 3:7. Meanwhile, in AM/MSN120, the characteristic peaks of crystalline AM were not observed at the ratio of 7:3, 5:5 and 3:7. The absence of characteristic diffraction peaks indicates that MSN entrapped almost all AM, and changes the molecular state of the compound from crystalline to amorphous.

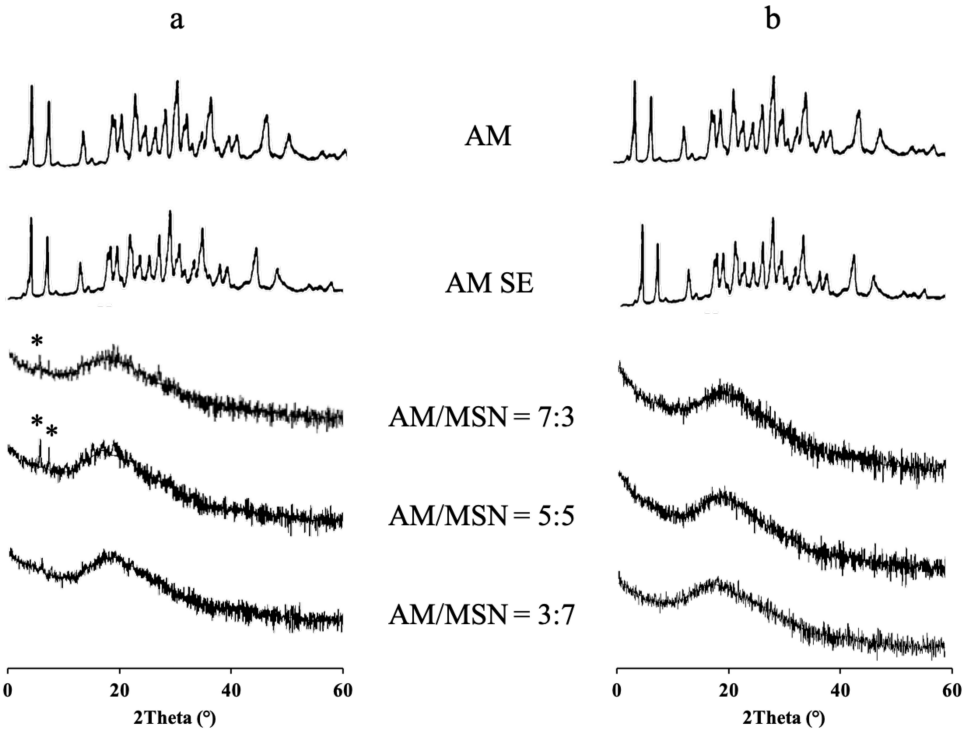

Figure 2 XRD pattern of (**a**) AM/MSN45 and (**b**) AM/MSN120 with various ratio. The asterisk represents the peaks of crystalline AM.

DSC Analysis

DSC analysis was conducted based on the presence of melting peaks to determine the maximum amount of AM loaded-MSN. The measurement result of AM/MSN45 and AM/MSN120 is presented in Figure 3. AM crystal and AM SE showed the endothermic melting peaks at 177 °C, while MSN did not feature any melting peak in DSC curves (data not shown). The peak of AM was still observed in AM/MSN at a weight ratio of 7:3 and 5:5 as well as in AM/MSN120 at a ratio of 7:3. The heat of fusion of AM decreased with a reduction in concentration of the compound in MSN, either in AM/MSN45 or AM/MSN120 system. Furthermore, the presence of a melting peak was attributed to the existence of some AM outside the MSN, which confirmed the result of the PXRD measurement.[23,38] In contrast, the peak was not observed in the AM/MSN45 = 3:7 and AM/MSN120 = 5:5. The absence was attributed to the successful encapsulation of AM into MSN.[39]

To confirm the relevance of loading amount with theoretical value, the calculation of AM/MSN45 and AM/MSN120, referred to as theoretical monolayer coverage of drug within MSN, were performed. Based on Equation (1), the amount of AM required for a monolayer coverage of MSN45 and MSN120 were 65.64 w/w% and 29.77 w/w%, respectively. The incorporation of 30% AM into MSN45 in the experiment was quite reasonable as it was lower than the theoretical value. This signified that AM was monomolecularly adsorbed on the silica surface of MSN4.[23] In contrast, the theoretical amount needed to fill the silica surface of MSN120 was significantly different compared to the AM-loaded-MSN120 obtained experimentally. The amount of AM obtained experimentally was significantly higher than that of the theoretical monolayer coverage value. Based on the assumption, the bigger pores of MSN120 should provide drug molecules more capacity, thus the AM can form the multilayers formation within MSN120.[40] Therefore, further investigation was needed to confirm the mechanism of AM within this mesoporous material. Based on this result, the theoretical calculation of AM is not adequate to estimate the maximum loading amount. The AM/MSN45 = 3:7 and AM/MSN120 = 5:5 were used for the subsequent FT-IR measurement, as well as dissolution and physical stability studies.

FT-IR Measurement

The carbonyl of AM presents electronegative oxygen centers, thus the interaction of AM and MSN can be predicted through hydrogen bonding between the electron's lone pairs associated with surface silanol groups. It is important to acknowledge that FT-IR measurement was utilized to evaluate the interaction between AM and the silica surface of MSN. Absorbed water was

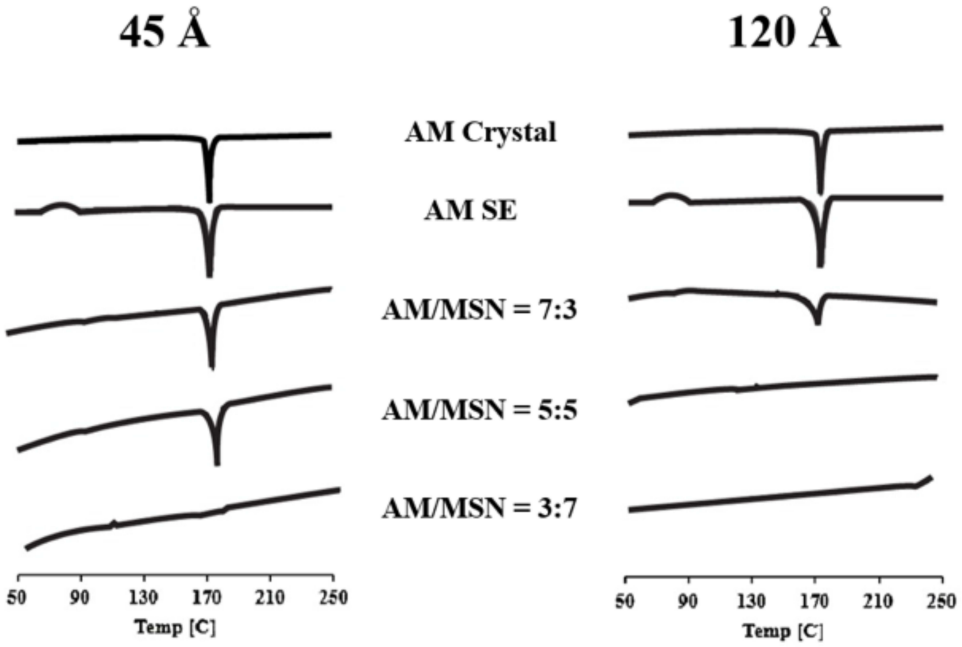

Figure 3 DSC pattern of AM, AM SE, and AM/MSN with various weight ratio.

https://doi.org/10.2147/NSA.S499007

identified as the cause of the infrared absorption peaks in the MSN45 spectra, which were located at around 1630 cm^{-1}, as presented in Figure 4. This result was in line with a previous study reporting adsorption peaks at these wavelengths.[41] In AM/MSN45, a free carbonyl vibration around 1632.77 cm^{-1} changed to 1631.81 cm^{-1}. This signified the possibility of the hydrogen bonding between the carbonyl oxygen atom of AM with the surface hydroxyl of MSN45. Similar results were also observed in the AM-loaded MSN120, a free carbonyl vibration changed to 1611.55 cm^{-1} (Figure 5). This indicated that the interaction between the silanol groups on the surface of MSN120 with the carbonyl group of AM was formed within the material.

Solubility Test

The solubility was measured to characterize the relative hydrophobicity of the AM. Using 50 mm phosphate buffer of pH 7.4 and at a temperature of 37 °C, the equilibrium solubility of AM was determined. The equilibrium level of crystalline AM value was identified at 0.43 ± 0.3 µg/mL, signifying the extremely poor aqueous solubility of the compound. Table 1 shows that the solubility was improved in the presence of MSN. The enhancement within MSN might be related to

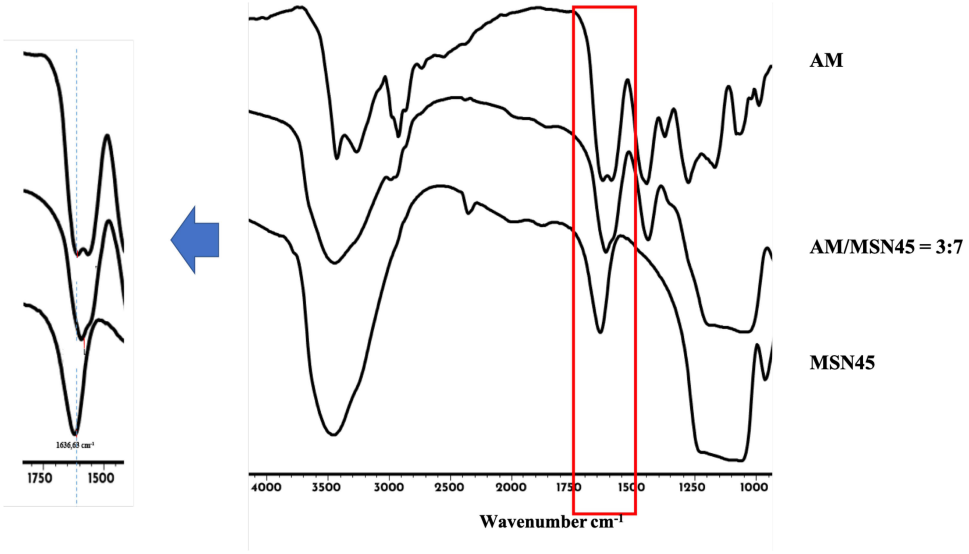

Figure 4 FT-IR results of AM, AM/MSN45, and MSN45.

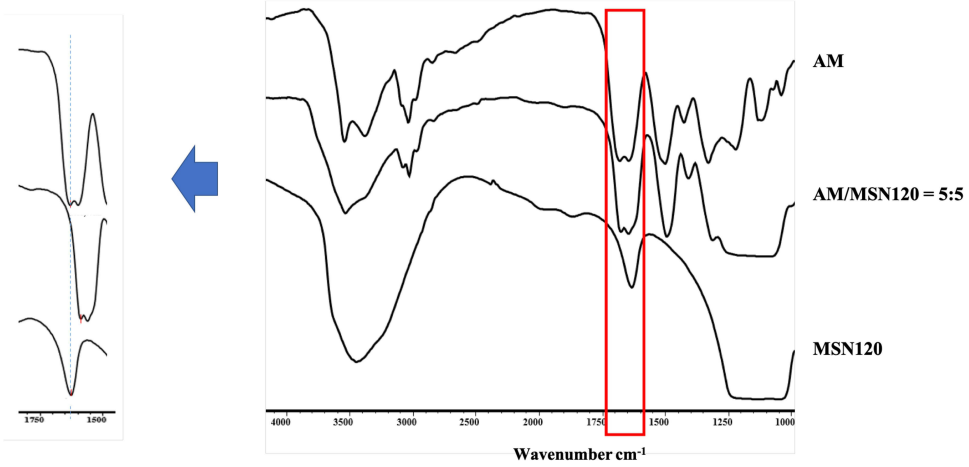

Figure 5 FT-IR spectra for AM, AM/MSN120, and MSN120.

https://doi.org/10.2147/NSA.S499007

Table 1 Crystalline ($S_{c,AM}$) and Amorphous ($S_{a,AM}$) Solubility of AM in 50 mm Phosphate Buffer at pH 7.4

Sample	$S_{c,AM}$ (µg/mL)	$S_{a,AM}$ (µg/mL)	$S_{a,AM}$ /$S_{c,AM}$
AM crystal	0.43 ± 0.3	0.43 ± 0.3	1
AM SE	0.43 ± 0.3	0.44 ± 0.06	1.02
AM/MSN45	0.43 ± 0.3	18.50 ± 6.49	43.02
AM/MSN120	0.43 ± 0.3	6.40 ± 0.22	14.88

several mechanisms including changing the physical state from a crystalline to an amorphous state, and particle size reduction due to monomolecularly dispersion.[23,39] However, amorphization could be the main reason for AM solubility enhancement. This is because the amorphous of the compound was stabilized by the nanoconfinement effect and surface interaction.[42]

Dissolution Test

The dissolution test of AM was performed in 50 mm phosphate buffer at pH 7.4 and 37 °C under non-sink conditions as shown in Figure 6.[19,43] The loading efficiency of AM/MSN45 was discovered to be 95.07% ± 0.36 (w/w, n = 3), while the efficiency of AM/MSN120 was 99.48% ± 1.18% (w/w, n = 3). The concentration of phosphate buffer used as the dissolution medium was 50 mm. Previous reports stated that the aggregation of molecules through hydrophobic interactions would be promoted by increasing ionic strength leading to a decrease in the coexistence of concentration.[19,43] The AM crystal showed a slow dissolution rate, and the concentration of the compound was determined at 0.43 ± 0.3 µg/mL. The dissolution profile of AM/MSN45 = 3:7 showed a rapid dissolution at the beginning of dissolution test and reached a maximum concentration of approximately 18.50 ± 6.49 µg/mL. Monomolecular dispersion of AM within MSN led to good dispersibility in the medium at the beginning of the test. The concentration of AM then gradually decreased due to associated nucleation and crystallization in the dissolution medium. Meanwhile, the AM dissolution of AM/MSN120 was considerably different compared to AM/MSN45. At the beginning of the test, the dissolution of AM in the AM/MSN120 was slower and reached the highest concentration of AM at 6.40 ± 0.22 µg/mL. Nevertheless, the concentration of AM in AM/MSN120 was still higher than that of AM crystal at approximately 0.44 µg/mL. This indicated that incorporating AM into MSN could improve AM dissolution. However, the difference in pore sizes between MSN and AM can have an impact on the dissolution profile.

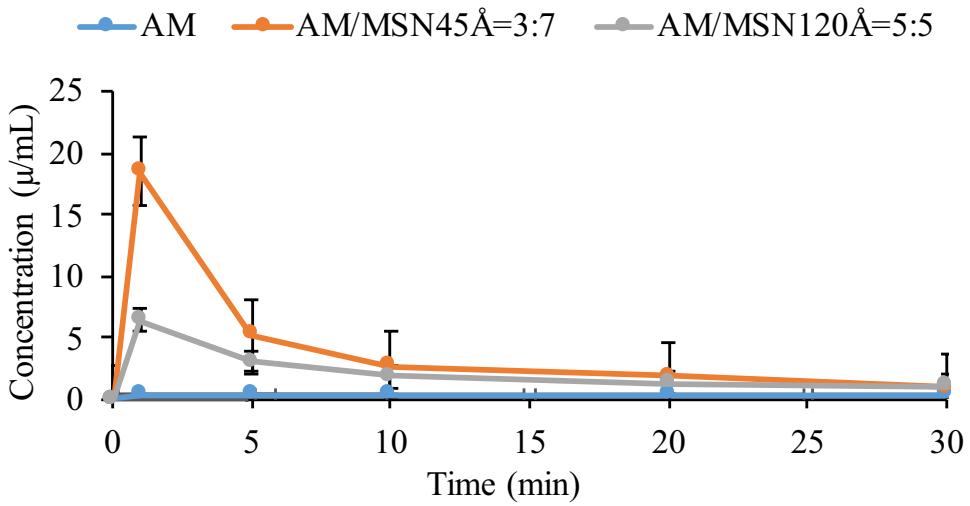

Figure 6 Dissolution profiles of AM crystal, AMMSN45=3:7, and AM/MSN120 5:5.

https://doi.org/10.2147/NSA.S499007

Physical Stability Test

Physical stability of the AM/MSN45 = 3:7, and AM/MSN120 = 5:5 were monitored from PXRD measurements, as presented in Figure 7. The characteristic peaks of crystalline AM were observed in AM/MSN45 = 3:7 recrystallized after 7 days of storage at 25 ºC and 95% RH, due to the recrystallization. Meanwhile, AM/MSN120 = 5:5 retained its amorphous state after 7 days of storage at 25 °C and 95% RH. However, after 14 days of storage, we observed the characteristic peaks of crystalline AM. These data indicated that AM recrystallization occurred in either MSN45 or MSN120. This could be due to the fact that in a humidified condition, the water will compete with the drug in the case of interaction with the surface of MSN; thus, the water will replace AM and occupy the surface of MSN, facilitating the easy escape of AM from MSN pores and leading to the recrystallization outside the material.

Discussion

Speculated mechanism of AM dissolution from AM/MSN45 = 3:7, and AM/MSN120 = 5:5 is summarized in Figure 8. Immediately after AM/MSN45 = 3:7 was dispersed into the dissolution medium (pH 7)., the dissolution medium directly entered into the pores of MSN45. In drug development, pH 7.4 is frequently chosen as the primary condition for examining dissolution and release behavior because of its physiological relevance, especially for intravenous administration. The systemic blood pH is rigorously maintained at around 7.4, rendering it an essential factor for assessing the pharmacokinetics of the drug post-absorption into the bloodstream. In the context of oral administration, despite the gastrointestinal tract's varying pH levels, the intestine is the primary site for drug absorption. The small intestine offers a significant surface area for absorption and has a longer transit time than the stomach, establishing it as the principal site for drug uptake. Focusing on dissolution and release at pH 7.4 provides a more precise prediction of the drug's bioavailability and therapeutic efficacy across various routes of administration. The monomolecularly dispersed AM on the surface of this mesoporous material can rapidly dissolve into the medium through the interaction of water molecules with the hydrophilic form of the compound. Therefore, the dissolved AM was rapidly released from the pore into the bulk medium. The high concentration of the compound was temporarily formed due to the rapid dissolution. The concentration then decreased because the crystal growth was formed in bulk solution. Meanwhile, in the case of AM/MSN120 = 5:5, the release of AM was lower compared to AM/MSN45 = 3:7. This is likely due to the formation of AM multilayers within the MSN, which may suppress the rapid release of IBCAM from the pores into the bulk dissolution medium. The multilayers formation of AM could suppress the water contacting to AM occupying the surface of MSN

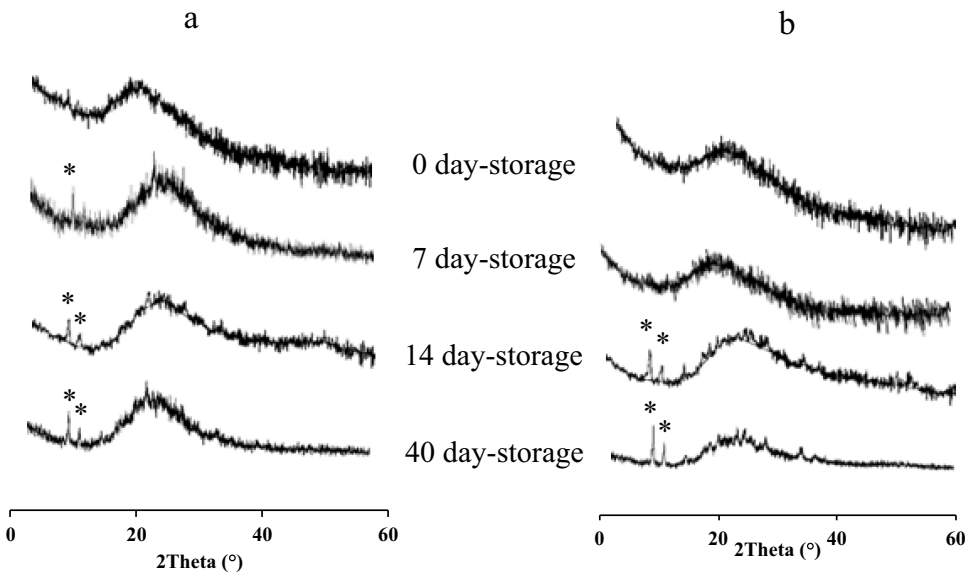

Figure 7 The PXRD pattern of a (**a**) AM/MSN45 = 3:7, AND (**b**) AM/MSN120 = 5:5 after storage at 25°C, 95%RH. The asterisk represents the peaks of crystalline AM.

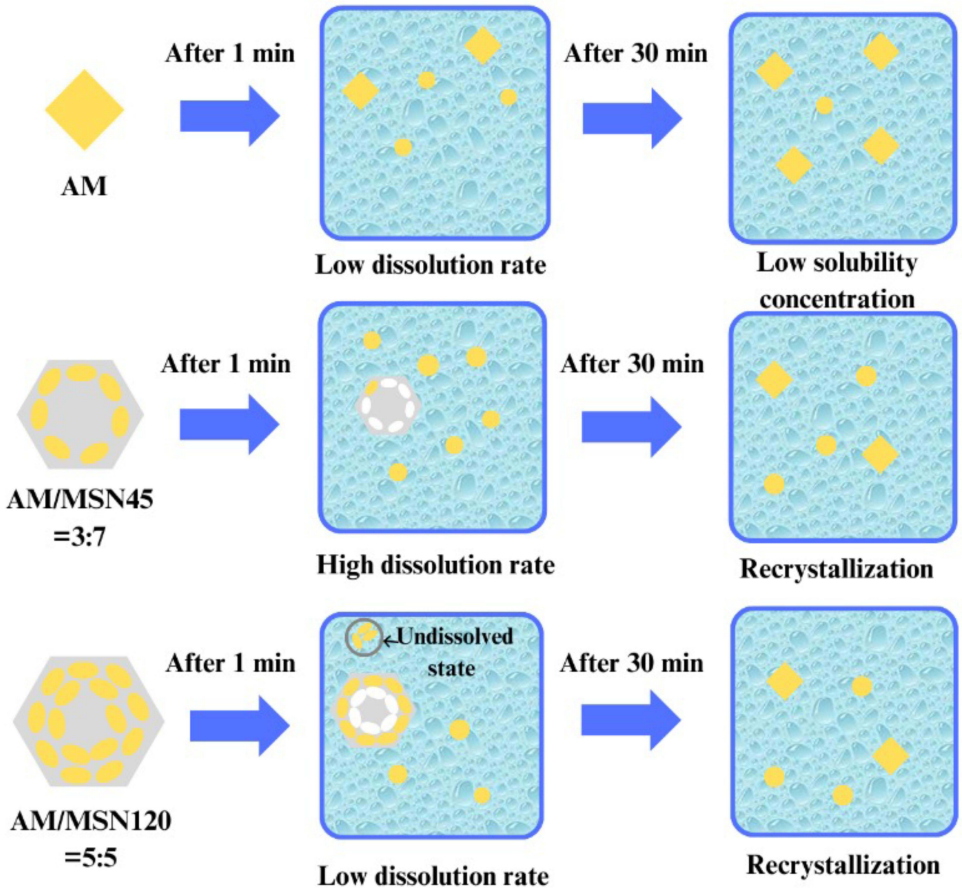

Figure 8 Schematic illustration of AM dissolution from AM/MSN45 = 3:7, and AM/MSN120 = 5:5.

due to the intermolecular interaction of AM within MSN120. Thus, the water only contact directly with the surface of multilayers formation of AM, leading to the low concentration of AM from AM/MSN120 compared to AM/MSN45.[43]

The mechanism of physical stability from AM/MSN45 = 3:7, and AM/MSN120 = 5:5 under humidified conditions was presented in Figure 8. Humidifying condition causes the absorption of water molecules by the surface of the drug, leading to recrystallization.[44] In the process, water enters into mesopores of MSN and interacts with the surface of the material. This led to the replacement interaction between the drug and the silanol group. The hydrophilic surfaces of MSN show stronger interactions with water compared to hydrophobic surfaces.[45,46] Therefore, water molecules can break hydrogen bonds between silanol groups and drugs when the relative humidity is high, facilitating the release of drugs. It is important to acknowledge that the existence of AM outside MSN can induce recrystallization. The drug molecules will recrystallize in the mesopores only when the pores size of the material is greater than 20 times the diameter of the molecule.[47] The pore size of MSN at 16 and 45 Å is approximately 4–12 times larger than the size of the AM of 11.76 Å × 9.20 Å. Therefore, recrystallization for AM/MSN45 = 3:7 and AM/MSN120 = 5:5 under humidifying conditions occurred in the outside of the material. The pore size of mesoporous silica nanoparticles (MSN) significantly affects the dissolution behavior and drug release profile of α-mangostin, as demonstrated by the differing release patterns for MSN45 and MSN120. The rapid dissolution and temporary high concentration in the bulk medium for AM/MSN45 can be attributed to the monomolecular dispersion of α-mangostin on the surface of smaller pores[48,49] The improved dissolution is likely attributed to the increased surface area and the close interaction with hydrophilic silanol groups, facilitating rapid release and transient supersaturation. The decrease in concentration resulting from crystallization in the bulk medium indicates that while smaller pores enhance dissolution rates, the preservation of supersaturation is temporary, constrained by nucleation and crystal growth processes.[50,51]

The slower release from AM/MSN120 underscores the influence of multilayer formation within the larger pores. The diminished release rate indicates that the aggregation of α-mangostin molecules within MSN120 forms a barrier that obstructs water penetration, thereby inhibiting rapid dissolution. This observation contrasts with the anticipated result, as larger pores generally promote quicker release, highlighting the significance of intermolecular interactions in regulating the dissolution process. Multilayer formation induces steric hindrance, which diminishes water accessibility and consequently restricts dissolution efficiency relative to the monomolecular dispersion seen in MSN45.[52]

The potential for recrystallization under humidified conditions supports the hypothesis that larger pores enhance crystallization beyond the mesopores. The pore sizes of MSN45 and MSN120 are 4–12 times larger than α-mangostin molecules, leading to recrystallization primarily occurring outside the mesopores. This phenomenon is attributed to the disruption of drug-silanol interactions by water molecules. This phenomenon reinforces the conclusion that pore size has a dual function in promoting initial dissolution and affecting the physical stability of the drug under particular environmental conditions.[53]

This study's observation of supersaturation behavior underscores the intricate relationship among pore size, dissolution rate, and recrystallization. MSN45 facilitates rapid and significant supersaturation, whereas MSN120 exhibits a more regulated, though reduced, release attributed to the multilayered structure of α-mangostin. The findings suggest that the supersaturation state is influenced not only by pore size but also by the molecular organization present within the pores.

The pore size of mesoporous silica nanoparticles affects the dissolution and release behavior of α-mangostin via mechanisms related to surface area, steric effects, and recrystallization potential. MSN45 enables rapid dissolution and transient supersaturation owing to its smaller pores and larger surface area, while MSN120's larger pores result in slower release due to multilayer formation and decreased water accessibility. This analysis offers a detailed perspective on the customization of mesoporous materials to improve drug release profiles and increase the bioavailability of poorly water-soluble compounds such as α-mangostin of mesoporous silica nanoparticles (MSN) significantly affects the dissolution behavior and drug release rate of α-mangostin through various physicochemical interactions. Smaller pores, as observed in MSN45, offer a greater surface area compared to MSN120. The increased surface area facilitates greater contact between α-mangostin and the dissolution medium, thereby promoting a more rapid initial dissolution and potentially leading to a heightened supersaturation state. Supersaturation is crucial for poorly water-soluble compounds such as α-mangostin, as it increases apparent solubility and may enhance bioavailability. Reduced pore sizes restrict drug molecule mobility, thereby decreasing the probability of rapid diffusion while facilitating sustained release via gradual diffusion over time.

Larger pores, exemplified by MSN120, diminish steric hindrance and facilitate accelerated drug diffusion owing to their more open structure, thereby enhancing the release rate. The rapid diffusion may induce a more immediate yet less stable supersaturation state, which could lead to a more rapid decrease in concentration upon reaching equilibrium. Larger pores elevate the risk of recrystallization, especially when their size substantially exceeds that of the α-mangostin molecules. The cited statement indicates that recrystallization typically occurs outside the mesopores when the pore size is more than 20 times the molecular diameter. The pore sizes of MSN45 (approximately 45 Å) and MSN120 (approximately 120 Å) are 4–12 times larger than that of α-mangostin (dimensions of 11.76 Å × 9.20 Å), indicating a greater potential for recrystallization in MSN120, especially in humid conditions. This would impair the dissolution and release performance by decreasing the quantity of amorphous α-mangostin available for rapid dissolution.

The behavior of supersaturation is closely related to pore size. In MSN45, α-mangostin is maintained in a highly dispersed, potentially amorphous state, which promotes prolonged supersaturation. The larger pores of MSN120 may enhance initial solubilization rates; however, they may also lead to a more rapid depletion of the supersaturated state due to recrystallization or swift diffusion into the surrounding medium. The pore size affects the dissolution rate and release, as well as the stability and duration of supersaturation, all of which are essential for optimizing the bioavailability of α-mangostin.

The interaction of pore size, surface area, steric effects, and recrystallization potential highlights the intricate dynamics of α-mangostin dissolution and release. MSN45 is more likely to maintain supersaturation and facilitate gradual release due to its increased surface area and confinement effects. In contrast, MSN120 may result in a quicker yet less stable dissolution profile, exhibiting a greater tendency for recrystallization and rapid depletion of the supersaturated

state.The physical stability of AM/MSN120 was observed to be greater due to the multilayers formation of AM within MSN120, which could suppress the release of AM from MSN. The primary mechanism through which mesoporous silica (MSN) enhances the physical stability of α-mangostin is its capacity to encapsulate drug molecules within its mesoporous structure, thereby diminishing the chances of recrystallization and aggregation.[53–56] The larger pore size in MSN120 promotes the formation of multilayers of α-mangostin within the mesopores. The multilayer formation is essential for improving physical stability by inhibiting the rapid release of α-mangostin into the surrounding medium. The close packing of drug molecules within the multilayers creates strong intermolecular interactions, such as van der Waals forces and hydrogen bonding, which further stabilize the amorphous state of α-mangostin. The limited mobility restricts the interaction between water molecules and the drug, consequently impeding the dissolution process and reducing the likelihood of recrystallization. The confined environment within MSN120 serves as a barrier to environmental factors like humidity, which can induce recrystallization, thus significantly improving the physical stability of α-mangostin over time.

Conclusion

In conclusion, the mechanism of the AM incorporated into MSN with various pore sizes and its relationship with dissolution properties and physical stability were elucidated. The AM was successfully incorporated into MSN through the solvent evaporation method, confirmed by PXRD and DSC measurements. FT-IR measurements showed that the hydrogen bond interaction between the carbonyl group of AM and the silanol surface of the mesoporous material was formed. The smaller pores size of MSN showed rapid release of AM in the dissolution medium and featured greater physical stability. This provided a fundamental insight into the formulation of the drug encapsulated into MSN, specifically in elucidating the relationship between the pore size of the MSN with the dissolution rate and physical stability of the amorphous drug.

Acknowledgments

We would like to thank Universitas Padjadjaran for APC.

Funding

This research was funded by the Universitas Padjadjaran (Riset Percepatan Lektor Kepala) to Diah Lia Aulifa (No. 1549/UN6.3.1/PT.00/2023).

Disclosure

The authors report no conflicts of interest in this work.

References

1. Ibrahim MY, Hashim NM, Mariod AA, et al. α-Mangostin from Garcinia mangostana Linn: an updated review of its pharmacological properties. *Arab J Chem*. 2016;9(3):317–329. doi:10.1016/j.arabjc.2014.02.011
2. Mohamed GA, Al-Abd AM, El-halawany AM, Abdallah HM, Ibrahim SRM. New xanthones and cytotoxic constituents from Garcinia mangostana fruit hulls against human hepatocellular, breast, and colorectal cancer cell lines. *J Ethnopharmacol*. 2017;198:302–312. doi:10.1016/j.jep.2017.01.030
3. Orozco FG, Chitchumroonchokchai C, Lesinski GB, Suksamrarn S, Failla ML. α-Mangostin: anti-inflammatory activity and metabolism by human cells. *J Agric Food Chem*. 2013;61(16):3891–3900. doi:10.1021/jf4004434
4. Syam S, Bustamam A, Abdullah R, et al. β Mangostin suppress LPS-induced inflammatory response in RAW 264.7 macrophages in vitro and carrageenan-induced peritonitis in vivo. *J Ethnopharmacol*. 2014;153(2):435–445. doi:10.1016/j.jep.2014.02.051
5. Asasutjarit R, Meesomboon T, Abulheem P, et al. Physicochemical properties of alpha-mangostin loaded nanomeulsions prepared by ultrasonication technique. *Heliyon*. 2019;5(9):1–11. doi:10.1016/j.heliyon.2019.e02465
6. Koh JJ, Qiu S, Zou H, et al. Rapid bactericidal action of alpha-mangostin against MRSA as an outcome of membrane targeting. *Biochim Biophys Acta*. 2013;1828(2):834–844. doi:10.1016/j.bbamem.2012.09.004
7. Sakagami Y, Piyasena MLKGNP, Dharmaratne HRW, Dharmaratne HRW. Antibacterial activity of α-mangostin against vancomycin resistant Enterococci (VRE) and synergism with antibiotics. *Phytomedicine*. 2013;12(3):203–208. doi:10.1016/j.phymed.2003.09.012
8. Chomnawang MT, Surassmo S, Nukoolkarn VS, Gritasanapan W. Effect of Garcinia mangostana on inflammation caused by Propionibacterium acnes. *Fitoterapia*. 2007;78(6):401–408. doi:10.1016/j.fitote.2007.02.019

9. Azimi H, Tafti MF, Khakshur AA, Abdollahi M. A review of phytotherapy of acne vulgaris: perspective of new pharmacological treatments. *Fitoterapia*. 2012;83(8):1306–1317. doi:10.1016/j.fitote.2012.03.026
10. Dreno B, Pecastaings S, Corvec S, Verald S, Khammari A, Roques C. Cutibacterium acnes (Propionibacterium acnes) and acne vulgaris: a brief look at the latest updates. *J Eur Acad Dermatol Venereol*. 2018;32(S2):5–14. doi:10.1111/jdv.15043
11. Platsidaki E, Dessinioti C. Recent advances in understanding Propionibacterium acnes (*Cutibacterium acnes*) in acne. *F1000Res*. 2018;7:1953. doi:10.12688/f1000research.15659.1
12. Asasutjarit R, Larpmahawong P, Fuongfuchat A, Sareedenchai V, Veeranonddha S. Physicochemical properties and anti-Propionibacterium acnes activity of film-forming solutions containing alpha-mangostin-rich extract. *AAPS Pharm Sci Tech*. 2013;15(2):306–316. doi:10.1208/s12249-013-0057-8
13. Pp I, Wongsomboon A, Kokpol C, Chaichanawongsaroj N, Wanichwecharungruang S. Depositing α-mangostin nanoparticles to sebaceous gland area for acne treatment. *J Pharmacol Sci*. 2015;129(4):226–232. doi:10.1016/j.jphs.2015.11.005
14. Budiman A, Megantara S, Apriliani A. Solid Dosage Form Development Of Glibenclamide-Aspartame Cocrystal using the Solvent Evaporation Method to Increase The Solubility of Glibenclamide. *Int J Appl Pharm*. 2021;2021:150–154.
15. Skorupska E, Jeziorna A, Potrzebowski MJ. Thermal Solvent-Free Method of Loading of Pharmaceutical Cocrystals into the Pores of Silica Particles: a Case of Naproxen/Picolinamide Cocrystal. *J Phys Chem*. 2016;120:13169–13180.
16. Wu W, Löbmann K, Schnitzkewitz J, et al. Aspartame as a co-former in co-amorphous systems. *Int J Pharm*. 2018;549(1–2):380–387. doi:10.1016/j.ijpharm.2018.07.063
17. Budiman A, Citraloka ZG, Muchtaridi M, Sriwidodo S, Aulifa DL, Rusdin A. Inhibition of Crystal Nucleation and Growth in Aqueous Drug Solutions: impact of Different Polymers on the Supersaturation Profiles of Amorphous Drugs-The Case of Alpha-Mangostin. *Pharmaceutics*. 2022;14(11):2386. doi:10.3390/pharmaceutics14112386
18. Budiman A, Rusdin A, Aulifa DL. Current Techniques of Water Solubility Improvement for Antioxidant Compounds and Their Correlation with Its Activity: molecular Pharmaceutics. *Antioxidants*. 2023;12(2):378. doi:10.3390/antiox12020378
19. Budiman A, Aulifa DL. A Comparative Study of the Pharmaceutical Properties between Amorphous Drugs Loaded-Mesoporous Silica and Pure Amorphous Drugs Prepared by Solvent Evaporation. *Pharmaceuticals*. 2022;15(6):730. doi:10.3390/ph15060730
20. McCarthy CA, Zemlyanov DY, Crean AM, Taylor LS. Comparison of Drug Release and Adsorption under Supersaturating Conditions for Ordered Mesoporous Silica with Indomethacin or Indomethacin Methyl Ester. *Mol Pharm*. 2020;17(8):3062–3074. doi:10.1021/acs.molpharmaceut.0c00489
21. Brouwers J, Brewster ME, Augustijns P. Supersaturating drug delivery systems: the answer to solubility-limited oral bioavailability? *J Pharm Sci*. 2009;98(8):2549–2572. doi:10.1002/jps.21650
22. Budiman A, Nurfadilah N, Muchtaridi M, Sriwidodo S, Aulifa DL, Rusdin A. The Impact of Water-Soluble Chitosan on the Inhibition of Crystal Nucleation of Alpha-Mangostin from Supersaturated Solutions. *Polymers*. 2022;14(20):4370. doi:10.3390/polym14204370
23. Budiman A, Aulifa DL. Encapsulation of drug into mesoporous silica by solvent evaporation: a comparative study of drug characterization in mesoporous silica with various molecular weights. *Heliyon*. 2021;7(12):e08627. doi:10.1016/j.heliyon.2021.e08627
24. Qian S, Heng W, Wei Y, Zhang J, Gao Y. Coamorphous Lurasidone Hydrochloride–Saccharin with Charge-Assisted Hydrogen Bonding Interaction Shows Improved Physical Stability and Enhanced Dissolution with pH-Independent Solubility Behavior. *Cryst Growth Des*. 2015;15(6):2920–2928. doi:10.1021/acs.cgd.5b00349
25. Bremmell KE, Prestidge CA. Enhancing oral bioavailability of poorly soluble drugs with mesoporous silica based systems: opportunities and challenges. *Drug Dev Ind Pharm*. 2019;45(3):349–358. doi:10.1080/03639045.2018.1542709
26. Andersson J, Rosenholm J, Areva S, Lindén M. Influences of Material Characteristics on Ibuprofen Drug Loading and Release Profiles from Ordered Micro- and Mesoporous Silica Matrices. *Chem*. 2004;16:4160–4167.
27. Vraníková B, Niederquell A, Šklubalová Z, Kuentz M. Relevance of the theoretical critical pore radius in mesoporous silica for fast crystallizing drugs. *Int J Pharm*. 2020;591:120019.
28. Antonino RSCMQ, Ruggiero M, Song Z, et al. Impact of drug loading in mesoporous silica-amorphous formulations on the physical stability of drugs with high recrystallization tendency. *Int J Pharm*. 2019;X(1):100026.
29. Bavnhøj CG, Knopp MM, Madsen CM, Löbmann K. The role interplay between mesoporous silica pore volume and surface area and their effect on drug loading capacity. *Int J Pharm*. 2019;X:1,100008.
30. Liao Y-T, Lee C-H, Chen S-T, Lai J-Y, KC-W W. Gelatin-functionalized mesoporous silica nanoparticles with sustained release properties for intracameral pharmacotherapy of glaucoma. *J Mater Chem B*. 2017;5(34):7008–7013. doi:10.1039/C7TB01217A
31. Luo L-J, Nguyen DD, Lai J-Y. Benzoic acid derivative-modified chitosan-g-poly (N-isopropylacrylamide): methoxylation effects and pharmacological treatments of glaucoma-related neurodegeneration. *J Control Release*. 2020;317:246–258. doi:10.1016/j.jconrel.2019.11.038
32. Price DA, Blagg J, Jones L, Greene N, Wager T. Physicochemical drug properties associated with in vivo toxicological outcomes: a review. *Expert Opin Drug Metab Toxicol*. 2009;5(8):921–931. doi:10.1517/17425250903042318
33. Yang C, Nguyen DD, Lai J. Poly(l-Histidine)-Mediated On-Demand Therapeutic Delivery of Roughened Ceria Nanocages for Treatment of Chemical Eye Injury. *Adv Sci*. 2023;10(26):26. doi:10.1002/advs.202302174
34. Young RJ. Physical properties in drug design. *Tactics in Contemporary Drug Design*. 2015;2015:1–68.
35. Azaïs T, Tourné-Péteilh C, Aussenac F, et al. Solid-State NMR Study of Ibuprofen Confined in MCM-41 Material. *Chem Mater*. 2006;18(26):6382–6390. doi:10.1021/cm061551c
36. Dening TJ, Taylor LS. Supersaturation Potential of Ordered Mesoporous Silica Delivery Systems. Part 1: dissolution Performance and Drug Membrane Transport Rates. *Mol Pharm*. 2018;15(8):3489–3501. doi:10.1021/acs.molpharmaceut.8b00488
37. Greenspan L. Humidity fixed points of binary saturated aqueous solutions. *J Res Natl Bur Stand a Phys Chem*. 1977;81A(89):89. doi:10.6028/jres.081A.011
38. Budiman A, Higashi K, Ueda K, Moribe K. Effect of drug-coformer interactions on drug dissolution from a coamorphous in mesoporous silica. *Int J Pharm*. 2021;600:1–11. doi:10.1016/j.ijpharm.2021.120492
39. Liu N, Higashi K, Kikuchi J, et al. Molecular-Level Understanding of the Encapsulation and Dissolution of Poorly Water-Soluble Ibuprofen by Functionalized Organic Nanotubes Using Solid-State NMR Spectroscopy. *J Phys Chem B*. 2016;120(19):4496–4507. doi:10.1021/acs.jpcb.6b00939
40. Moritz M, Geszke-Moritz M, Gorantla S, Singhvi G. Mesoporous Materials as Elements of Modern Drug Delivery Systems for Anti-Inflammatory Agents: a Review of Recent Achievements. *Pharmaceutics*. 2022;15(1):14. doi:10.3390/pharmaceutics15010014

41. Tozuka Y, Wongmekiat A, Kimura K, Moribe K, Yamamura S, Yamamoto K. Effect of pore size of FSM-16 on the entrapment of flurbiprofen in mesoporous structures. *Chem Pharm Bull*. 2005;53(8):974–977. doi:10.1248/cpb.53.974
42. Bavnhøj CG, Knopp MM, Löbmann K. Effect of Drug Loading in Mesoporous Silica on Amorphous Stability and Performance. *Pharmaceutics*. 2024;16(2):163. doi:10.3390/pharmaceutics16020163
43. Ilevbare GA, Taylor LS. Liquid–Liquid Phase Separation in Highly Supersaturated Aqueous Solutions of Poorly Water-Soluble Drugs: implications for Solubility Enhancing Formulations. *Cryst Growth Des*. 2013;13(4):1497–1509. doi:10.1021/cg301679h
44. Dhondale MR, Thakor P, Nambiar AG, et al. Co-Crystallization Approach to Enhance the Stability of Moisture-Sensitive Drugs. *Pharmaceutics*. 2023;16(1):15. doi:10.3390/pharmaceutics16010015
45. Pantale C, Senesi R, Andreani C, et al. Interaction of single water molecules with silanols in mesoporous silica. *Phys Chem Chem Phys*. 2011;13(13):6022–6028. doi:10.1039/c0cp02479a
46. Weinberger C, Zysk F, Hartmann M, et al. The structure of water in silica mesopores – influence of the pore wall polarity. *Advanced Materials Interfaces*. 2022;9(20):2200245. doi:10.1002/admi.202200245
47. Ambrogi V, Perioli L, Marmottini F, Giovagnoli S, Esposito M, Rossi C. Improvement of dissolution rate of piroxicam by inclusion into MCM-41 mesoporous silicate. *Eur. J. Pharm. Sci.* 2007;32(3):216–222. doi:10.1016/j.ejps.2007.07.005
48. Peng S, Huang B, Lin Y, Pei G, Zhang L. Effect of surface functionalization and pore structure type on the release performance of mesoporous silica nanoparticles. *Microporous Mesoporous Mater*. 2022;336:111862. doi:10.1016/j.micromeso.2022.111862
49. Shafiee M, Abolmaali S, Abedanzadeh M, Abedi M, Tamaddon A. Synthesis of pore-size-tunable mesoporous silica nanoparticles by simultaneous sol-gel and radical polymerization to enhance silibinin dissolution. *Iran J Med Sci*. 2021;46(6):475. doi:10.30476/ijms.2020.86173.1595
50. Candela-Noguera V, Alfonso M, Amorós P, Aznar E, Marcos MD, Martínez-Máñez R. In-depth study of factors affecting the formation of MCM-41-type mesoporous silica nanoparticles. *Microporous Mesoporous Mater*. 2024;363:112840. doi:10.1016/j.micromeso.2023.112840
51. Lin C-Y, Yang C-M, Lindén M. Dissolution and morphology evolution of mesoporous silica nanoparticles under biologically relevant conditions. *J Colloid Interface Sci*. 2022;608:995–1004. doi:10.1016/j.jcis.2021.09.164
52. Iraji S, Ganji F, Rashidi L. Surface modified mesoporous silica nanoparticles as sustained-release gallic acid nano-carriers. *J Drug Deliv Sci Technol*. 2018;47:468–476. doi:10.1016/j.jddst.2018.08.008
53. Kamarudin NHN, Jalil AA, Triwahyono S, et al. Variation of the crystal growth of mesoporous silica nanoparticles and the evaluation to ibuprofen loading and release. *J Colloid Interface Sci*. 2014;421:6–13. doi:10.1016/j.jcis.2014.01.034
54. Bore MT, Pham HN, Switzer EE, Ward TL, Fukuoka A, Datye AK. The role of pore size and structure on the thermal stability of gold nanoparticles within mesoporous silica. *J Phys Chem B*. 2005;109(7):2873–2880. doi:10.1021/jp045917p
55. El Mourabit S, Guillot M, Toquer G, Cambedouzou J, Goettmann F, Grandjean A. Stability of mesoporous silica under acidic conditions. *RSC Adv*. 2012;2(29):10916–10924. doi:10.1039/c2ra21569a
56. Gabaldon JP, Bore M, Datye AK. Mesoporous silica supports for improved thermal stability in supported Au catalysts. *Top Catal*. 2007;44(1–2):253–262. doi:10.1007/s11244-007-0298-4